Light driven magnetic transitions in transition metal dichalcogenide heterobilayers

IOP Publishing Journal of Physics: Condensed Matter
J. Phys.: Condens. Matter **35** (2023) 095801 (15pp) https://doi.org/10.1088/1361-648X/acab49

Light driven magnetic transitions in transition metal dichalcogenide heterobilayers

Michael Vogl[1,*], **Swati Chaudhary**[2,3,4] **and Gregory A Fiete**[3,4]

[1] Department of Physics, King Fahd University of Petroleum and Minerals, 31261 Dhahran, Saudi Arabia
[2] Department of Physics, The University of Texas at Austin, Austin, TX 78712, United States of America
[3] Department of Physics, Northeastern University, Boston, MA 02115, United States of America
[4] Department of Physics, Massachusetts Institute of Technology, Cambridge, MA 02139, United States of America

E-mail: ssss133@googlemail.com

Received 18 October 2022, revised 22 November 2022
Accepted for publication 13 December 2022
Published 23 December 2022

Abstract

Motivated by the recent excitement around the physics of twisted transition metal dichalcogenide (TMD) multilayer systems, we study strongly correlated phases of TMD heterobilayers under the influence of light. We consider both waveguide light and circularly polarized light. The former allows for longitudinally polarized light, which in the high frequency limit can be used to selectively modify interlayer hoppings in a tight-binding model. We argue based on quasi-degenerate perturbation theory that changes to the interlayer hoppings can be captured as a modulation to the strength of the moiré potential in a continuum model. As a consequence, waveguide light can be used to drive transitions between a myriad of different magnetic phases, including a transition from a 120′ Neel phase to a stripe ordered magnetic phase, or from a spin density wave phase to a paramagnetic phase, among others. When the system is subjected to circularly polarized light we find that the effective mass of the active TMD layer is modified by an applied electromagnetic field. By simultaneously applying waveguide light and circularly polarized light to a system, one has a high level of control in moving through the phase diagram in-situ. Lastly, we comment on the experimental feasibility of Floquet state preparation and argue that it is within reach of available techniques when the system is coupled to a judiciously chosen bath.

Keywords: moiré, transition metal dichalcogenide, Floquet, non-equlibrium, magnetism, phase transitions, non-equilibrium

(Some figures may appear in colour only in the online journal)

* Author to whom any correspondence should be addressed.

1. Introduction

Recent years have seen an explosion of interest in so-called moiré materials [1–5]. These are materials in which two dimensional crystals are stacked in such a way that their lattices interfere to form moiré patterns. In the earliest works related to such a material—twisted bilayer graphene (TBG)—the moiré patterns appear due to a relative twist between two graphene layers and have been found to lead to flat bands near a 'magic angle' [6–8]. It was speculated that this could lead to various strongly correlated phases, because flat bands imply tiny kinetic energy making any weak electron-electron interaction energy dominant [9–17].

In 2018 interaction driven phases in flat band systems were experimentally confirmed when superconductivity and insulating phases in TBG were reported [18]. Since then there have been theoretical predictions and experimental discoveries of a plethora of different strongly correlated phases [18–32]. These phases can range from various magnetic states [29–32] to superconducting states [29, 30]. This discovery naturally leads to the question of which related materials may harbor similarly exciting properties.

One such material class that has recently risen to popularity is bilayer or few layer transition metal dichalcogenides (TMDs) with a relative twist between layers [33–42]. Similar to TBG, theory has predicted [36–38, 40, 41] and experiment has confirmed [42, 43] there exists a zoo of strongly correlated phases. Analogously to TBG, these phases can be tuned via the twist angle. Compared to TBG, the twisted TMD systems offer the addition degree of freedom of material choice used to build the moiré heterostructure which can be used to tune different phases of matter. Recently, it was shown theoretically that TMD heterobilayers possess very rich phase diagrams that include a multitude of different magnetically ordered phases [36].

While TMD heterostructures might seem more complicated than graphene based multilayer materials (each TMD layer corresponds to three atomic layers), effective descriptions for TMD heterostructures can be significantly simpler than TBG because the former allow for an effective single band description that mimics a two-dimensional non-relativistic single particle Schrödinger equation with a periodic potential originating in the moiré patterns [36–38, 44]. This is in stark contrast to the case of graphene based moiré materials such as TBG, where one needs a four component Hamiltonian similar to a massless Dirac equation to describe layer and sublattice pseudo-spin degrees of freedom. It is worth mentioning, however, that recently, the dimensionality of the TBG Hamiltonian for a chiral limit has been reduced to a $2 \sim 2$ Hamiltonian in an approach where the Hamiltonian is squared [45, 46]. Nevertheless, for TBG a mapping from position dependent interlayer hoppings to an effective potential and a single band description is problematic. In fact, such a mapping has only been made rigorously for a closely related effective one-dimensional case, where moiré patterns are due to a stretch of one of the layers [47–49]. Even in this case, the argument only applies semiclassically. It is the simplicity of effective Hamiltonians for the TMD heterobilayers that motivates us to focus on the engineering of phase transitions for this class of materials, rather than TBG.

The TMD heterobilayer platform can be made even more manipulable by combining it with Floquet engineering which has been touted as a very powerful technique to modify the properties of quantum systems with light. In this technique, periodic drives are used to induce different material properties in a so-called prethermal phase that bears resemblance to an equilibrium phase. Recent years have witnessed incredible progress both on the theoretical as well as the experimental side of Floquet engineering. Specifically, on the theoretical side, there has been progress on estimating how long (given certain assumptions to driving strengths and frequencies) one can remain in the prethermal regime, which is often exponentially long [50, 51].

There has been tremendous progress in the development of techniques that facilitate effective time-independent descriptions using so-called effective Floquet Hamiltonians [50, 52–77]. Importantly, there has also been progress in our understanding of how to prepare prethermal Floquet phases [78–80]. For instance, it is now better understood what properties a bath has to fulfill for a system to relax into a so-called Floquet-Gibbs state [78, 79, 81], which can tell us much about how to prepare the ground state of a Floquet Hamiltonian. In addition to the work on the theoretical foundations of Floquet engineering, there have been predictions of a multitude of exciting light induced properties and phases of matter [82–135] (see [136, 137] for a recent review article). Recently, Floquet engineering is gaining popularity in moiré materials—albeit in the non-interacting limit [134–148].

In this work, we make a first step towards Floquet engineering of different phases of matter in *interacting* moiré materials. To maximize the accessibility of our results, we will focus on a simplified approach using a model description of a twisted TMD heterobilayer. This will allow us to focus on the universal features expected in experiment. A schematic depiction of the experimental scenario we envision can be seen in the figure 1.

Our paper is organized as follows. First, in section 2 we give a brief review of the effective Hamiltonian used to model TMD heterobilayers. Then, in section 3 we briefly describe the techniques used to derive interaction terms for an effective lattice model and discuss how a specific form of light, waveguide light possessing a longitudinal polarization, can be used to target specific parameters of the non-interacting limit. Similarly, we show that circularly polarized light can be employed to tune the effective mass of the active TMD layer, which also appears in the non-interacting limit. A central result of our work is that by tuning the properties and type of incident light one can reach a multitude of vastly different magnetic phases of matter in a twisted TMD without the need to change the specifics of the sample, such as the twist angle or constituent TMDs. One achieves dramatic control over the phase diagram. Finally, in section 4 we finish with a discussion on how specifics of the environment determine how 'Floquet ground state' phases can be prepared in practice. We conclude in section 5.

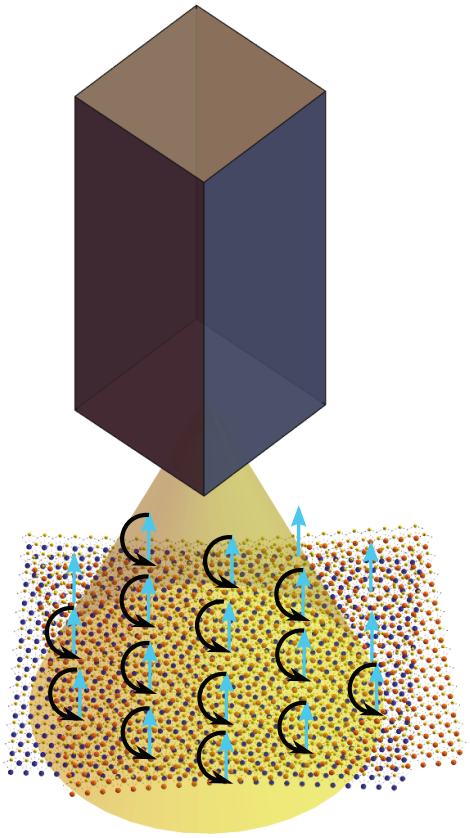

Figure 1. Schematic representation of how the magnetic ground state of a twisted TMD heterobilayer placed at the exit of a waveguide (illustrated as a dark rectangular prism) can be affected by light emanating from the waveguide. For example, the light might cause some of the spins to reorient themselves. Blue and orange spheres correspond to transition metal atoms, yellow ones to chalcogenides. The two layers have a relative twist, as shown. Spins are represented in light blue.

2. Model

We consider a generic non-interacting model [36–38]

$$H[\quad \frac{\hbar^2\mathbf{k}^2}{2m^\circ};\ 2\Lambda)\mathbf{x}+, \tag{1}$$

for 'electrons' in a TMD heterobilayer such as $WSe_2/MoSe_2$ or WSe_2/MoS_2. In this model, electrons are constrained to move in only one of the transition metal layers–the so-called active layer (AL). This means that additional layers that appear in such a TMD heterostructure are only taken into account via the effective potential $\Lambda)\mathbf{x}+$and mass m°. Some interaction effects are taken into account on a density functional theory (DFT) level because these models are typically fit to DFT band structures. Furthermore, it is important to stress that the model is coarse-grained, losing some short distance features. It is most accurate at long wavelengths, specifically near the point of a single TMD layer [37].

Electronic excitations in this model have an effective mass of $m^\circ \approx 0.5m_e$, where m_e is the bare electron mass (details depend crucially on the type of heterobilayer, whether $WSe_2/MoSe_2$ or WSe_2/MoS_2 or something else). For a twisted bilayer with small twist angle the effective periodic potential $\Lambda)\mathbf{x}+$has a six-fold rotational symmetry due to moiré patterns that appear from the interference between the two lattices. It is given as [36–38]

$$\Lambda)\mathbf{x}+[\quad V_m\Big[\quad \cos)\mathbf{b}_i\mathbf{x};\ \psi+, \tag{2}$$

where V_m is the strength of this potential and typically $V_m \approx 10\,\mathrm{meV}$. Here, the $\mathbf{b}_i$ are the three shortest reciprocal lattice vectors for the moiré lattice that are related by a $120'$ rotation and ψ is a phase shift that is determined by band structure fits.

As described in [36, 149], strong correlation effects for twisted TMDs can be included in a simple approximation where Wannier wavefunctions are determined using the non-interacting model equation (1) only. These Wannier wavefunctions can then be used to compute effective hopping terms on the moiré lattice, Hubbard-U-like interaction terms, etc. Therefore, much of the interacting structure is crucially influenced by the properties of the non-interacting underlying model. In some cases approximations can even be found by analytical means. For instance, it has been shown that one may approximate the potential equation (2) by a harmonic potential [38]. Harmonic oscillator wavefunctions then act as reasonably accurate approximations to the actual Wannier functions [38] and computations of Hubbard-U-like interaction terms can be done analytically, offering much insight [38].

The most important point we would like to emphasize is that the interaction parameters will depend on the parameters of the non-interacting model–particularly the moiré potential strength V_m. This observation is especially lucid in the case of the work by Hu and MacDonald [36], where only one of the axes in their interacting phase diagram (see figure 3) depends on V_m. This observation serves as motivation for the next section.

3. Light induced engineering of phase transitions

In this section, motivated by the work of Hu and MacDonald [36], we focus on how to engineer magnetic phase transitions by using two types of light. First we consider light emanating from a waveguide and afterwards the more standard case of circularly polarized light.

For light eminating from a waveguide the starting point of our discussion is a generic tight binding model. Here, the influence of light can be included through the hopping terms t_{ij} according to the Peierls substitution

$$t_{ij} \leftrightarrow e^{\int_{\mathbf{r}_i}^{\mathbf{r}_j}\mathbf{A}(t)*d\mathbf{l}}t_{ij}, \tag{3}$$

where $\mathbf{A}$ is the vector potential. Note that if one shines *normally incident longitudinally polarized light* onto a multilayered material only interlayer couplings are affected by this substitution (for in-plane hoppings the scalar product $\mathbf{A})t+\times d\mathbf{l}$ vanishes). Such an exotic form of light can be found at the exit

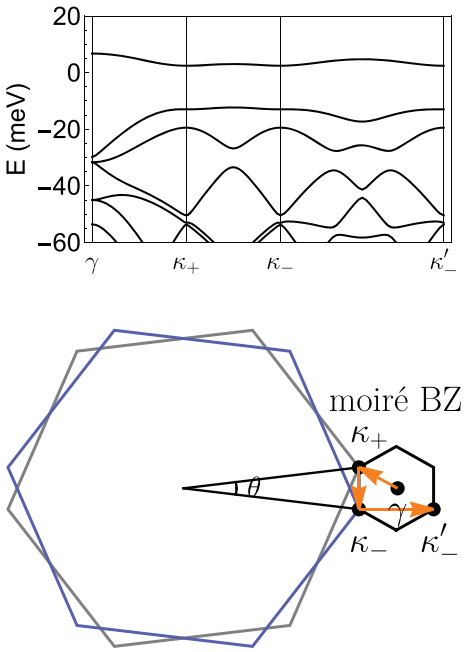

Figure 2. Top: plot of the non-interacting band-structure for $V_m = 6.6\,\text{meV}$, $m^* = 0.35m_e$, $a_M = 12\,\text{nm}$ and $\psi = -94°$. Bottom: the moire Brillouin zone along with the path that was taken for the bandstructure plot marked in orange.

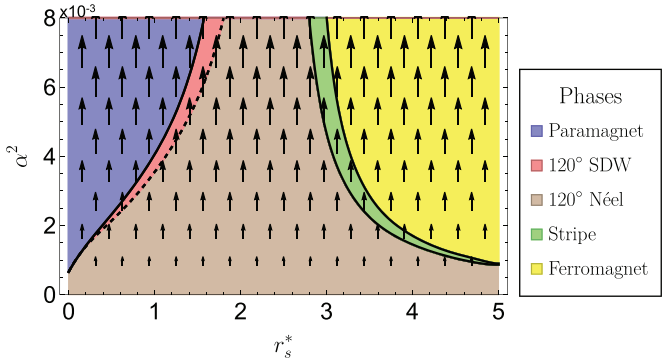

Figure 3. Adapted and modified redrawn version of the phase diagram from [36]. Different magnetic phases in a twisted TMD are shown in different colors. Black arrows to indicate how waveguide light can allow one to tune vertically across phase boundaries in the phase diagram. The parameter α^2 appearing in equation (6) is increased as V_m is decreased, according to equation (5).

of a waveguide [145], where it is allowed due to cavity boundary conditions.

It was shown in [145] that in the high frequency limit (the light frequency is larger than the bandwidth of the bands of interest but smaller than be bandgap) the effective time-independent interlayer couplings t_{ij} given by

$$t_{ij} \leftrightarrow J_0)a_{\text{L}}A\text{+}t_{ij}, \tag{4}$$

where J_0 is the zeroth Bessel function of the first kind that modulates the hopping amplitude. Here, a_{L} is the interlayer distance and A the strength of the incident light beam (constants like $\hbar$, etc are absorbed into A).

The time-averaged Peierls result, equation (4), can be exploited to modify couplings in equation (1). First, one realizes that the non-interacting bands are relatively flat as noted in [36–38]. The bands for which the harmonic oscillator wavefunctions hold as an accurate approximation of Wannier wavefunctions are especially flat, which can also be seen quite clearly in the figure 2 below. The flat band around the Fermi level energetically separated from other bands means that we can reasonably employ the high frequency approximation discussed above.

Instead of taking equation (1) as a starting point for the description of a twisted TMD one could also take a tight binding model that includes both TMD layers as a starting point. This type of model could be downfolded into an effective tight binding model that only includes the AL–the inactive layers (ILs) would be integrated out–employing a quasi-degenerate perturbation theory such as a Schrieffer–Wolff transformation or Loewdin downfolding. In this case, the dominant (2nd order in perturbation theory) contribution from interlayer tunnelings would be hopping processes like AL $\leftrightarrow$ IL $\leftrightarrow$ AL, assuming that the dominant interlayer hopping strengths are small compared to the dominant intralayer hoppings. Since hopping terms typically decrease exponentially with distance, the most dominant process is where the initial point on the AL is the same as (right 'above') the final point on the AL.

Hopping processes with different initial and final points on the AL would contribute as an effective or indirect intralayer hopping, which we will neglect because direct intralayer hoppings can be expected to be much larger. This means that the dominant effect of interlayer hopping leads to on-site potential terms like $\epsilon_i \tilde{c}_i\, c_i$, where the onsite energies $\epsilon_i \mathcal{P}\, t_{ij}^2$. A slightly more rigorous treatment of these ideas for the example of a 1D chain can be found in appendix A. In the language of the continuum model, on-site energies can be translated as a smoothed potential. In our case, this means that effective on-site energies that are due to second order interlayer hopping processes can be identified as the dominant origin of the moiré potential in equation (1).

In the high frequency limit when the material is subjected to the waveguide light

$$V_m \leftrightarrow)J_0)a_{\text{L}}A\text{+}\tilde{V}_m, \tag{5}$$

where a_{L} is a parameter taken to be $0.85a_{\text{TT}}$, the order of the distance between two transition metal layers a_{TT}. (see appendix B.) Equation (5) can now directly be used to move in the phase diagram shown in figure 3. Specifically, one may introduce the following parameters [36]

$$\begin{aligned} r_s^\circ &[\left(\frac{1}{\epsilon}\right)\frac{3}{4\pi^2}\left\langle^{1/4}\frac{a_M}{a_B}\frac{m^\circ}{m}, \\ \alpha^2 &[\frac{\hbar^2}{m^\circ \beta V_m a_M^2}, \end{aligned} \tag{6}$$

where m is the bare electron mass, m° the effective mass, $a_B [\frac{\epsilon\hbar^2}{e^2 m}$ the Bohr radius, a_M the moiré lattice constant, $\beta [16\pi^2 \cos)\psi\text{+}$a material dependent numerical constant (material dependent through ψ appearing in equation (2)–we assume

the case $\pi/3 < \psi < \pi/3$) and ε the dielectric constant. The quantity $a_B r_s^\circ$ can be interpreted as the typical distance between electrons [36]. Approximating the wells of the moiré potential by a local harmonic potential, α can be related to a harmonic oscillator length scale.

A typical twisted TMD might have parameters $a_M \gg 10$ nm, m° [0.3 m, ε [10, $V_m \gg 30$ meV, from which we get $r_s^\circ \gg 2.97$ and $\alpha^2 \gg 5.98 \sim 10^{\ 3}$, placing one near the boundary of a stripe and FM region (see figure 3). Therefore, it may be possible to tune different phases in a twisted TMD hetero bilayer with relative ease. Indeed, in our case one is able to change V_m (without additional effects in the high frequency regime) by applying waveguide light. More precisely, one can directly tune α^2, equation (6), increasing it in size, since V_m is reduced according to equation (5). The effect of this can be seen below in figure 3.

While the phase boundaries are the same as in [36], our original contribution is the addition of arrows that show how the coupling parameters α^2 and r_s° are renormalized under the drives we consider. For instance, this allows us to show that tuning V_m indirectly through the influence of light one can drive phase transitions, such as from a 120′ Neel phase to a stripe ordered phase or to a ferromagnetic phase, for example. Note that shifting phases becomes easier as the harmonic oscillator length scale α is increased because for a small change to $V_m \leftrightarrow V_m \quad \delta V$ we have $\alpha^2 \leftrightarrow)\alpha^{\dagger}\neq^2 \gg \alpha^2$; $\alpha^2 \frac{\delta V}{V_m}$. We emphasize the crucial point that the drives we consider do not change the phase diagram, but allow one to experimentally tune between phases within it. Such a situation is rare in driven systems.

Within our model, waveguide light only allows one to tune parameter the α. However, one can gain greater control over the phase diagram of a twisted TMD by tuning the second parameter, r_s°, which can be done with circularly polarized light modeled by a vector potential $\mathbf{A}$ [$A)\cos)\omega t+,\sin)\omega t++$ We note that r_s° can be tuned by such a choice of vector potential because it depends on the effective mass m° in the active TMD layer—a parameter that is primarily determined by values of in-plane hopping elements of a tight binding model. Circularly polarized light is a good choice if one aims to modify m° because it primarily influences the in-plane hopping elements. Typically, the most relevant out-of-plane hopping elements are almost directly perpendicular to the plane of the material and therefore they are influenced very little by circularly polarized light (recall the details of the Peierls substitution and that circularly polarized light only has in-plane vector potential components that are non-zero)—indeed hopping elements decay rapidly with distance.

Before we discuss the effect of circularly light on the effective mass m° in equation (1), we first note that the quadratic dispersion that appears in equation (1) can be an approximation valid near different high-symmetry points in the hexagonal Brillouin zone. Indeed, depending on the precise choice of TMD material, low energy electrons might either be close to the K points [37] or the point [44]. In both cases, near those points the band structure can be approximated by a quadratic dispersion.

Table 1. Mass renormalization parameter Λ near the Γ point computed based on effective third nearest neighbor tight binding with parameters that were taken from [150]. We also compare results that were obtained using different approximations to the exchange correlation potential of DFT: generalized gradient (GGA) and local density approximation (LDA). These different approximations were used in [150] to fit a third nearest neighbor tight binding model, which we used in our computations. Details of the computation to determine those parameters are found in appendix C.

Active layer	Λ (GGA)	Λ (LDA)
MoS_2	0.998	1.338
WS_2	1.021	1.183
$MoSe_2$	1.556	1.334
WSe_2	0.332	1.530
$MoTe_2$	8.219	1.070
WTe_2	1.366	1.203

Since and K points are separated by a large distance in k-space, electrons at each of these points can be treated as independent excitations as noted in the appendix of [39]. In what follows we will therefore investigate the impact of circularly polarized light on the effective masses of the lowest energy band near the and K points. In addition, we will highlight the differences at the and K points. Here, it suffices to restrict our investigation to the impact on the active TMD layer.

First, we investigate the effect of circularly polarized light on excitations near the point. Our starting point is a third nearest neighbor three-band tight binding model [150] of a TMD that we discuss in more detail in appendix C. From this model we find that circularly polarized light in the high frequency limit (frequencies larger than the bandwidth) modifies the effective mass m° as

$$m^\circ \leftrightarrow)1\,; \quad \Xi a^2 A^2 \dashv m^\circ, \tag{7}$$

where we assumed a relatively weak field strength A, and a is the in-plane lattice constant. A mass renormalization parameter Ξ that describes how strongly the effective mass m° is increased due to the electromagnetic field strength A depends on the particular choice of active TMD layer. Values of Ξ for a variety of active TMD layer choices are given below in table 1.

We find that most computed values of the renormalization parameter Ξ are close to unity. However, Ξ seems to be more strongly dependent on a specific choice of tight binding model rather than the actual underlying material. Therefore, our results based on the tight binding parameters from [150] can be taken as an order of magnitude estimate. That is, we can only make the observation that circularly polarized light increases the effective mass near the point roughly as $m^\circ \leftrightarrow)a\,; \quad a^2 A^2 \dashv m^\circ$. Additional DFT based work might be necessary to find more reliable results for the mass renormalization parameter Ξ. Such an analysis is beyond the scope of the present work.

Despite the spread of values for Ξ we find that circularly polarized light allows one to manipulate r_s°, and therefore gain a high level of control over the phase diagram of [36]. Particularly, in figure 4 one can see how one may move in

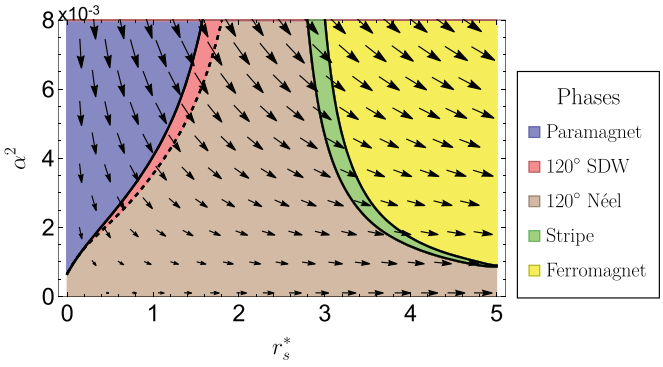

Figure 4. Adapted and modified redrawn version of the phase diagram from [36]. Different magnetic phases in a twisted TMD are shown in different colors. Black arrows indicate schematically how circularly polarized light can allow one to tune vertically across phase boundaries in the phase diagram. Due to the modifications that circularly polarized light enacts on the effective mass m^*, the parameter $\alpha^2 \to \alpha^2(1-a^2A^2)$ decreases depending on its position in the plot and the parameter $r_s^* \to r_s^*(1+a^2A^2)$ increases based on its position in the plot, which we indicated by arrows pointing along $(r_s^* a^2A^2, -\alpha^2 a^2A^2)$.

the phase diagram by the application of circularly polarized light.

From the phase diagram in figure 4 it becomes clear that circularly polarized light provides an additional knob that allows one to tune the magnetic phases of a twisted TMD heterobilayer independently from the tuning in the case of light emanating from a waveguide. We stress that while the phase diagram itself is unmodified from [36], in our theoretical treatment we were able to capture renormalized couplings that allow one to tune an experimental system along the arrows we have added to the phases diagram. The arrows, an original contribution of this work, can be interpreted as the couplings α^2 and r_s° flowing with increasing strength of the circularly polarized light.

Next, we turn to the effect of circularly polarized light on excitations near the K point. We investigate how it can also be used here to modify the effective mass m°. Here, we worked with a simpler nearest neighbor three band model for a TMD that was found in [150] so that a more concise analytical expression could be obtained in appendix D. We were able to do so because the simpler model is a good fit to the band structure near the K point—unlike the case of the point. The model and details of our computation are discussed in the appendix D. Relevant for the main text is the case of weak field strengths A and momenta near the K point. Similar to momenta near the point, we find that mass is renormalized as in equation (7). The renormalization parameters Ξ for a variety of materials are given in table 2.

We find that unlike the case of the point, circularly polarized light reduces the effective mass near the K point. The effect is generally not as pronounced as near the point, with a noticeably smaller $\Xi < 1$. The effect of circularly polarized light on effective masses seems to have a much stronger material dependence than in the case near the K point. Lastly, results

Table 2. Mass renormalization parameter Λ near the K point computed based on nearest neighbor tight binding models that were taken from [150]. Different DFT procedures such as generalized gradient (GGA) and local density approximation (LDA) were used to fit a nearest neighbor tight binding model. Details of the computation to determine parameter Λ are given in appendix D.

Active layer	Λ (GGA)	Λ (LDA)
MoS_2	−0.0550	−0.0507
WS_2	−0.0065	+0.0002
$MoSe_2$	−0.1674	−0.1701
WSe_2	−0.0937	−0.0858
$MoTe_2$	−0.4771	−0.5122
WTe_2	−0.3710	−0.3597

from different DFT approaches are in much better agreement with one another than in the case near the point. This might be attributed to less free parameters that appear in the nearest neighbor tight binding, which could guarantee a more consistent fit.

Interestingly, the mass is renormalized differently near the K and points. This observation could be used as an indirect probe to determine if certain material properties are dominated by the electrons near the K or points. That is, if we are near a phase transition point circularly polarized light might cause a phase transition in a case dominated by the point but not the K point or vice versa. This effect should be observable in magnetic response functions, most obviously the order parameter.

For completeness we note that the phase diagram in figure 3 (derived in [36]) made use of self-consistent Hartree–Fock theory for a further simplified lattice model. The full interacting Hamiltonian–including the Coulomb interaction $U)\mathbf{r}+$ was projected onto the highest band in figure 2. Therefore, the interactions were modeled by a generalized Hubbard term

$$H_{\text{int}} [\quad \frac{1}{2} \quad [\quad U)\mathbf{R} \quad \mathbf{R}^\dagger + c_{\mathbf{R},\tau} c_{\mathbf{R}',\tau'} c_{\mathbf{R}',\tau'} c_{\mathbf{R},\tau}, \qquad (8)$$

$\tau,\tau',\mathbf{R},\mathbf{R}'$

where $U)\mathbf{R} \quad \mathbf{R}^\dagger +$ corresponds to the Coulomb interaction evaluated using Wannier functions corresponding to moire lattice sites at positions $\mathbf{R}$ and $\mathbf{R}^\dagger$ [37].

4. Comments on Floquet state preparation

In the previous sections, we focused on how a periodic drive can modify exchange interactions in a TMD heterobilayer effective Hamiltonian. Our analysis was limited to studying the ground state magnetic properties of an effective time-independent Hamiltonian. However, the question about when the dynamics of the system can be fully described by this Floquet Hamiltonian is a very challenging one in itself and cannot be fully answered by direct studies of the properties of this Hamiltonian. Furthermore, it is an open problem, in general, how specific states of a Floquet Hamiltonian can be prepared experimentally. The answers to both these questions also depend on many other additional factors which include

the methods used to turn on a periodic drive and also the details of a coupling of the system to its environment. This means that there are various time scales that enter the problem. We briefly discuss some of these time-scales relevant to our proposal.

The first case we consider is one where an experimental setup allows preparation of an eigenstate of the Floquet Hamiltonian. It is well known that isolated Floquet systems due to interaction effects tend to heat to infinite temperature and thus it is challenging to keep an eigenstate of a Floquet Hamiltonian stable once it is attained. That is, the time evolution is only for a limited time governed by effective Floquet Hamiltonians—the so-called prethermal regime. After this regime a Floquet state will not be an eigenstate and therefore it will not be stable under time evolution. Nonetheless, generically, even interacting systems can sustain an exponentially long prethermal regime [50] before heating dynamics take over. Sufficiently weak drives in the high frequency regime permit some rough estimates of prethermal regime times $t_{\text{pre}}\,\mathcal{P}\exp)\omega/J+$ which can be made on the basis of interaction strength J and drive frequency ω [50]. However, not only is the length of the pre-thermal regime of experimental relevance, but also the length of time before the onset of the pre-thermal regime. The time required for the onset of the pre-thermal regime can be roughly estimated from the strength J of interactions, and is roughly of order $1/J$ [151] in this case.

The second case we consider is the problem of Floquet state preparation. While there does not seem to be a general route to prepare a Floquet state, an adiabatic switch-on protocol can be used to prepare Floquet states [152] if the initial state is adiabatically connected to the target state. An alternative route to the preparation of ground states of a Floquet Hamiltonian is via coupling to a heat bath. Particularly, it has been shown [78] that a periodically driven system under certain assumptions about the system-bath couplings will evolve into a so-called Floquet-Gibbs state. That is, the density matrix for relatively long times will evolve to be the density matrix for a Gibbs state $e^{\ \beta H_{\text{F}}}$, where H_{F} is the Floquet Hamiltonian [78]. This kind of state can be achieved under the condition that the heating rate of the driven system is smaller than the relaxation rate associated with the system-bath coupling. From this perspective the problem of Floquet state preparation can be shifted to a question about the engineering of appropriate system-bath couplings. However, there are also time scales involved with how long it takes to reach a Floquet-Gibbs state. To our knowledge there do not yet exist simple estimates for this time scale.

We will therefore focus on the time scales that we can estimate with current techniques. The prethermal regime can be achieved within a few 100 fs for $J \approx 10$ meV [151]. High-power ultrashort lasers with pulse widths of a few 100 fs are capable of generating electric field amplitudes in the range 0.1–1 V nm ^{1} [153]. This results in sufficiently large driving strengths to induce a magnetic phase transition if the system is close to a phase boundary. We conclude this section by noting that while it is challenging to apply our approach to tune magnetic phases in a twisted TMD, it is within current experimental reach.

5. Conclusion

In this work, we discussed how a periodic drive can be used to control and alter the magnetic properties of TMD heterobilayers. Many previous works [127–135] have studied light-induced modification in exchange interactions. Most of these changes originate from the direct modulation of in-plane hopping arising from the transverse **E** field of a laser. However, in our case, we harness the additional layer degree of freedom possessed by moiré materials and use waveguide light to get an **E** field perpendicular to the TMD layers. In this case, we take an indirect route to modify exchange interactions. The longitudinal field of the laser renormalizes interlayer hoppings which in turn leads to a modification of the moiré potential. This change affects interaction parameters and in turn the magnetic properties. Our scheme differs from previous proposals in that it is based on modifications to interaction parameters that arise from interlayer hopping renormalizations.

We have also studied the effect of circularly polarized light and found that it leads to a renormalization of the effective mass. This renormalization makes it possible to tune a separate parameter that determines the magnetic phase diagram. Circularly polarized light therefore serves as an additional tuning knob that allows one a high level of control over the phase diagram of a twisted TMD.

We note that an interesting future direction would be to study the effect of linearly polarized transverse light on the phase diagram, which due to the breaking of rotational symmetry could lead to a wealth of new different magnetic phases.

With the rapidly expanding zoo of moiré materials and their magnetic properties only scarcely understood at this point, we believe these methods would find many applications in this new class of materials. Furthermore, we believe that longitudinal light can find novel applications beyond Floquet engineering. For example, it would be interesting to explore the interplay of longitudinal waveguide light and moiré materials in the context of other light-matter phenomena such as optical responses, by generalizing the work of [154–156].

Data availability statement

All data that support the findings of this study are included within the article (and any supplementary files).

Acknowledgments

M V gratefully acknowledge the support provided by the Deanship of Research Oversight and Coordination (DROC) at King Fahd University of Petroleum & Minerals (KFUPM) for funding this work through start up Project No. SR211001 and subsequent continued funding through exploratory research Grant No. ER221002. This research was primarily supported by the National Science Foundation through the Center for Dynamics and Control of Materials: an NSF MRSEC under Cooperative Agreement No. DMR-1720595, with additional support from Grant No. DMR-2114825. G A F also acknowledges support from the Alexander von Humboldt Foundation.

Appendix A. Mechanism for on-site energy from interlayer hopping

In this appendix we will discuss in more detail the mechanism for indirect on-site hopping that eventually leads to the moiré potential in equation (1).

For simplicity of the discussion, let us consider a one dimensional system of two initially disjoint chains denoted by A and B:

$$H_0 = H_A + H_B + \sum_i \varepsilon_A a_i^\dagger a_i + t_A a_{i+1}^\dagger a_i + \text{h.c.} + \sum_i \varepsilon_B b_i^\dagger b_i + t_B b_{i+1}^\dagger b_i + \text{h.c.} \tag{A1}$$

with $\varepsilon_B \to \varepsilon_A$ and $\varepsilon_B - \varepsilon_A \to t_A, t_B$. That is the system has a relatively large energy gap, which makes it possible to find a simpler model by separating the problem into high- and low-energy sectors. We will be interested in the low-energy sector of this Hamiltonian, which is spanned by:

$$|k_a\rangle = a_k^\dagger |0\rangle = \sum_j e^{ikj} a_j^\dagger |0\rangle, \tag{A2}$$

with energy $E_k^a = \varepsilon_A + 2t_A \cos k$. The corresponding high-energy sector is spanned by

$$|k_b\rangle = b_k^\dagger |0\rangle = \sum_j e^{ikj} b_j^\dagger |0\rangle, \tag{A3}$$

with energy $E_k^b = \varepsilon_B + 2t_B \cos k$.

Now, we will consider the impact that a coupling between the two chains will have. Particularly, let us consider a perturbation arising from a site-dependent interchain hopping. Let's assume that the spatial dependence of this interchain hopping has a period $n > 1$. We can model this term as:

$$V = \sum_i t_{AB}^i a_i^\dagger b_i + \text{h.c.} + \sum_i v^i a_i^\dagger b_i + \text{h.c.}, \tag{A4}$$

with $v^{i+n} = v^i$. This perturbation is clearly off-diagonal between Θ_A and Θ_B where Θ_A and Θ_B are projection operators for chain A and B, respectively. Furthermore, the periodic nature of this perturbation allows us to write:

$$v^m = \sum_q e^{i\frac{2\pi m}{n} q} v_q. \tag{A5}$$

Now, we are interested in finding out how this perturbation affects the effective low-energy Hamiltonian. Here, we can employ a Schrieffer–Wolff transformations to derive the effective low-energy Hamiltonian. The second-order correction is given by:

$$H_{\text{eff},2} = \frac{1}{2} P_A [S_1, V] P_A, \tag{A6}$$

where

$$S_1 = \sum_{k',k} \frac{|k_a'\rangle\langle k_a'| V |k_b\rangle\langle k_b|}{E_{k'}^a - E_k^b} |k_a'\rangle\langle k_b| - \frac{|k_b\rangle\langle k_b| V |k_a'\rangle\langle k_a'|}{E_k^b - E_{k'}^a} |k_b\rangle\langle k_a'|. \tag{A7}$$

Now,

$$\langle k_a'| V |k_b\rangle = V_{k'k}^{ab} = \sum_j e^{i(k-k')j} v^j = \sum_{j,q} e^{i(k-k'+\frac{2\pi}{n}q)j} v_q = \left(\sum_q \delta\right) k - k' = \frac{2\pi}{n} q \rangle\rangle v_q, \tag{A8}$$

and equivalently

$$\langle k_b| V |k_a'\rangle = V_{kk'}^{ba} = \sum_j e^{i(k'-k)j} v^j = \sum_{j,q} e^{i(k'-k+\frac{2\pi}{n}q)j} v_q = \left(\sum_q \delta\right) k' - k = \frac{2\pi}{n} q \rangle\rangle v_q, \tag{A9}$$

$$H_{\text{eff},2}^{aa} = \frac{1}{2} \sum_{k'',k',k} \frac{V_{k'k}^{ab} V_{kk''}^{ba}}{E_{k'}^a - E_k^b} + \frac{V_{k'k}^{ab} V_{kk''}^{ba}}{E_k^b - E_{k''}^a} \langle k_a''| \rangle k_a'^\dagger, \tag{A10}$$

$$H_{\text{eff},2}^{aa} = \frac{1}{2} \sum_{k'',k',k,q,q'} \frac{1}{E_{k'}^a - E_k^b} \delta \left) k'^\dagger - k \right) \frac{2\pi}{n} q \rangle\rangle \sim \delta \left) k - k'' \right) k''^\dagger - k' \frac{2\pi}{n} q' \rangle\rangle v_q v_{q'} \langle k_a''| \rangle k_a'^\dagger + \frac{1}{2} \sum_{k'',k',k,q,q'} \frac{1}{E_k^b - E_{k''}^a} \delta \left) k'^\dagger - k \right) \frac{2\pi}{n} q \rangle\rangle \sim \delta \left) k - k'' \right) k''^\dagger - k' \frac{2\pi}{n} q' \rangle\rangle v_q v_{q'} \langle k_a''| \rangle k_a'^\dagger, \tag{A11}$$

$$H_{\text{eff},2}^{aa} = \frac{1}{2} \sum_{k,q,q'} \frac{1}{E_{k+\frac{2\pi}{n}q}^a - E_k^b} v_q v_{q'} \Big[\sim \Big(k; \frac{2\pi}{n} q \Big\langle_a \Big\rangle \Big) k \quad \frac{2\pi}{n} q' \Big\langle_a \Big(\Big(; \frac{1}{2} \sum_{k,q,q'} \frac{1}{E_k^a - \frac{2\pi}{n} q' - E_k^b} v_q v_{q'} \Big[\sim \Big(k; \frac{2\pi}{n} q \Big\langle_a \Big\rangle \Big) k \quad \frac{2\pi}{n} q' \Big\langle_a \Big(\Big(\tag{A12}$$

$$\Big(\Big(k; \frac{2\pi}{n} q \Big\langle_a \Big\rangle \Big) k \quad \frac{2\pi}{n} q' \Big\langle_a \Big(\Big([\sum_{l,m} e^{ik(l-m)} e^{i\frac{2\pi}{n}(ql+q'm)} l_q| \rangle m_a. \tag{A13}$$

For the case, where $\varepsilon_B \to \varepsilon_A, t_A, t_B$, we can simply assume $E_{k'}^a - E_k^b \gg \varepsilon_B$.

$$H_{\text{eff},2}^{aa} = \frac{1}{\varepsilon_B} \sum_{k,q,q',l,m} v_q v_{q'} e^{ik(l-m)} e^{i\frac{2\pi}{n}(ql+q'm)} l_q| \rangle m_a, \tag{A14}$$

$$H^{aa}_{\mathrm{eff},2} [\quad \frac{1}{\varepsilon_B} \Big[_{q,q',l,m} v_q v_{q'} \delta_{lm} e^{i\frac{2\pi}{n}(ql+q'm)} \; l_q| \rangle m_a \Big\rangle$$
$$[\propto H^{aa}_{\mathrm{eff},2} [\quad \frac{1}{\varepsilon_B} \Big[_{q,q',l} v_q v_{q'} e^{i\frac{2\pi}{n}(q+q')l} \; l_q| \rangle l_a \Big\rangle . \tag{A15}$$

Now, using equation (A5), we can show

$$H^{aa}_{\mathrm{eff},2} [\quad \frac{1}{\varepsilon_B} \Big[_l \Big) \underbrace{\Big[_q e^{i\frac{2\pi}{n}ql} v_q}_{v^l} \Big[\Big) \underbrace{\Big[_{q'} e^{i\frac{2\pi}{n}q'l} v_q^\dagger}_{v^l} \sum \Big\rangle \; l_q| \rangle l_a \Big\rangle$$
$$[\quad \Big[_l \frac{)v^l +^2}{\varepsilon_B} \Big\rangle \; l_q| \rangle l_a \Big\rangle \tag{A16}$$

which is an on-site energy shift proportional to the square of inter-layer at the given site. In second-quantization picture, we can write:

$$H_{\mathrm{eff},2} [\quad \Big[_i \frac{)t^i_{AB} -^2}{\varepsilon_B} a_i \, a_i . \tag{A17}$$

We notice the on-site potential is modified only at sites where interchain hopping is non-zero. These results can be simply generalized for a two-dimensional set up where we can just replace index i with a pair of indices i,j denoting the lattice site as long as we have a tight-binding Hamiltonian with nearest-neighbor interaction only.

Appendix B. Neglected effects of indirect hopping on-site potential

In our discussion we have focused on just two layers of the twisted TMD. However, it is important to note that a TMD bilayer does not consist of two atomic layers but actually six. In the example of $WSe_2/MoTe_2$ one has a layer structure like $Se \;\; W \;\; Se \;\; Te \;\; Mo \;\; Te$. For concreteness we will keep referring to the material combination $WSe_2/MoTe_2$, although for a general discussion one may take W/Mo as being any two different transition metals M and Se/Te as any chalcogenide X. If we now assume that W is the AL [38] we can then see that both hoppings $W \Rightarrow Te$ and $W \Rightarrow Mo$ contribute to the interlayer hopping that can lead to moiré potential $\Lambda)\mathbf{x}+$ It is therefore not completely correct to just replace $V_m \leftrightarrow J_0)a_{\mathrm{L}}A-^2$ because there is not just one interlayer lattice constant a_{L}. However, for the purposes of a clear discussion and to find a simplified and easy to interpret model we will make the approximation $a_{\mathrm{L}} [\;\; ca_{W \;\; Mo}$, which essentially boils down to an order of magnitude estimate. We can estimate that $c \approx 0.85$.

The reason for this approximation is as follows: First we see that the spacing between the centers of two TMD layers is approximately 6 Å [157]. Next, we note that the spacing between two the layers of M and X in a TMD MX_2 is approximately 1.5 Å [158, 159]. Therefore, if the hopping $W \Rightarrow Mo$ and $W \Rightarrow Te$ for the closer of the Te is dominant then both interlayer distances are somewhere between $0.7a_{W \;\; Mo}$ and $1a_{W \;\; Mo}$. Therefore, a compromise is $a_{\mathrm{L}} [\;\; 0.85a_{W \;\; Mo}$. This approximation will lead to small errors of $\lesssim$5% if we compare $J_0)a_{\mathrm{L}}A-^2$ to $J_0)_{W \;\; Mo}A-^2$ or $J_0)_{W \;\; Te}A-^2$ if driving strengths in the range $a_{\mathrm{L}}A < 0.5$ are considered.

Appendix C. Downfolding the three band model of a TMD subjected to circularly polarized light in the high frequency limit near the point

In this appendix, we study the impact of circularly polarized light on a twisted TMD hetero bilayer. We are interested in the effective mass near the point. Since circularly polarized light mostly modifies in-plane hopping elements we first consider the case of an isolated TMD layer, which in our case is assumed to describe the active TMD layer in our twisted TMD heterobilayer. The starting point of our discussion is the third nearest neighbor three band tight binding model of a TMD that was derived in [150]. The Hamiltonian is

$$H^{\mathrm{TNN}})\mathbf{k}+[\Big) \begin{matrix} V_0 & V_1 & V_2 \\ V_1^\circ & V_{11} & V_{12} \\ V_2^\circ & V_{12}^\circ & V_{22} \end{matrix} \Big\rangle \sum . \tag{C1}$$

This Hamiltonian is written in the basis of d-orbitals $\}d_{z^2}, d_{xy}, d_{x^2 \;\; y^2}\langle$. The different contributions to the Hamiltonian are given as

$$V_0 [\;\; \varepsilon_1 \,; \;\; 2t_0)2\cos X_k \cos Y_k \,; \;\; \cos 2X_k + \;\; ; \;\; 2r_0)2\cos 3X_k \cos Y_k \,; \;\; \cos 2Y_k + \;\; ; \;\; 2u_0)2\cos 2X_k \cos 2Y_k \,; \;\; \cos 4X_k + \tag{C2}$$

$$V_1 [\quad 2 \;\; \bar{3}t_2 \sin X_k \sin Y_k \,; \;\; 2)r_1 \,; \;\; r_2 + \sin 3X_k \sin Y_k \quad 2 \;\; \bar{3}u_2 \sin 2X_k \sin 2Y_k \;\; ; \;\; i\Big] 2t_1 \sin X_k)2\cos X_k \,; \;\; \cos Y_k + ; \;\; 2)r_1 \quad r_2 + \sim \sin 3X_k \cos Y_k \,; \;\; 2u_1 \sin 2X_k)2\cos 2X_k \,; \;\; \cos 2Y_k + \tag{C3}$$

$$V_2 [\;\; 2t_2)\cos 2X_k \quad \cos X_k \cos Y_k + \;\; \frac{2}{\bar{3}})r_1 \,; \;\; r_2 + \sim)\cos 3X_k \cos Y_k \quad \cos 2Y_k + ; \;\; 2u_2 \sim)\cos 4X_k \quad \cos 2X_k \cos 2Y_k + \;\; ; \;\; i\Big] 2 \;\; \bar{3}t_1 \cos X_k \sin Y_k \,; \;\; \frac{2}{\bar{3}} \sin Y_k)r_1 \quad r_2 + \sim)\cos 3X_k \,; \;\; 2\cos Y_k + ; \;\; 2 \;\; \bar{3}u_1 \cos 2X_k \sin 2Y_k \Big\rangle \tag{C4}$$

$$V_{11} [\;\; \varepsilon_2 \,; \;\;)t_{11} \,; \;\; 3t_{22} + \cos X_k \cos Y_k \,; \;\; 2t_{11} \cos 2X_k \;\; ; \;\; 4r_{11} \cos 3X_k \cos Y_k \,; \;\; 2)r_{11} \,; \;\; \bar{3}r_{12} + \cos 2Y_k \;\; ; \;\;)u_{11} \,; \;\; 3u_{22} + \cos 2X_k \cos 2Y_k \,; \;\; 2u_{11} \cos 4X_k , \tag{C5}$$

$$V_{12}\,[\;\;\overline{3})t_{22}\;\;\;t_{11}+\sin X_k\sin Y_k\,;\;\;4r_{12}\sin 3X_k\sin Y_k$$
$$;\;\;\overline{3})u_{22}\;\;\;u_{11}+\sin 2X_k\sin 2Y_k$$
$$;\;\;i\Big]4t_{12}\sin X_k)\cos X_k\;\;\;\cos Y_k+;\;\;4u_{12}\sin 2X_k$$
$$\sim)\cos 2X_k\;\;\;\cos 2Y_k+ \tag{C6}$$

with the shorthand

$$X_k\,[\;\;\frac{1}{2}k_x a=\;\;Y_k\,[\;\;\frac{\overline{3}}{2}k_y a. \tag{C7}$$

The different couplings ε_i, t_i, r_i and u_i for a variety of different TMDs can be found in [150].

Starting from this Hamiltonian circularly polarized light is introduced in the standard way via a vector potential $\mathbf{A})t+[$ $A)\cos)\omega t+,\sin)\omega t++$and employing the minimal substitution procedure $\mathbf{k}\leftrightarrow\mathbf{k}\,;\;\;\mathbf{A}$. This allows us to define

$$H)\mathbf{k},t+[\;\;H^{\mathrm{TNN}})\mathbf{k}\,;\;\;\mathbf{A})t++. \tag{C8}$$

In the high frequency limit to leading order we may include the effect of circularly polarized light by employing an average Hamiltonian procedure

$$H_{\mathrm{av}})\mathbf{k}+[\;\;\frac{1}{T}\int_0^T \mathrm{d}tH)\mathbf{k},t+, \tag{C9}$$

which corresponds to the leading order approximation of various high frequency expansions [55, 136].

The resulting Hamiltonian $H_{\mathrm{av}})\mathbf{k}+$includes various Bessel function factors $J_0)aA+,\;J_0)\;\;\overline{3}aA+$and $J_0)2aA+$but offers few insights and is unwieldy. Therefore, we do not explicitly include this expression here. However, it is important to note that it is diagonal at the point, $\mathbf{k}\,[\;\;$. Therefore, one may apply second order perturbation theory in $\mathbf{k}$ to determine the effective mass m° of the lowest band from a comparison to the energy expression $E\,[\;\;c\,;\;\;\frac{\hbar}{2m^*}k^2$ (small non-rotationally symmetric parts were dropped since they do not appreciably modify the band structure). A plot of such an approximation is shown in figure 5 below.

The same procedure can of course also be applied in the case of no circularly polarized light, $A\,[\;\;0$. Doing so one may find how light modifies the effective mass m°. In particular one finds the expression

$$\frac{m^\circ)A+}{m^\circ)A\,[\;\;0+}[\;\;1\,;\;\;\Xi a^2A^2, \tag{C10}$$

where we have employed an expansion for small field strengths A. An explicit expression for Ξ is given below:

$$\Xi\,[\;\;\frac{1}{4}\Big)\frac{9)r_1\;\;\;r_2\,;\;\;t_1\,;\;\;2u_1+\frac{2}{}\;\;6r_0\;\;\;6r_{11}\;\;\;2\;\;\overline{3}r_{12}\,;\;\;2t_0\;\;\;t_{11}\;\;\;t_{22}\,;\;\;8u_0\;\;\;4u_{11}\;\;\;4u_{22}|}{6r_0\,;\;\;6r_{11}\,;\;\;2\;\;\overline{3}r_{12}\;\;\;6t_0\,;\;\;3t_{11}\,;\;\;3t_{22}\;\;\;6u_0\,;\;\;3u_{11}\,;\;\;3u_{22}\;\;\;\varepsilon_1\,;\;\;\varepsilon_2|^2}$$
$$;\;\;\frac{27)r_1\;\;\;r_2\,;\;\;t_1\,;\;\;2u_1+\frac{2}{}\;\;18r_0\;\;\;18r_{11}\;\;\;4\;\;\overline{3}r_{12}\,;\;\;6t_0\;\;\;3t_{11}\;\;\;3t_{22}\,;\;\;24u_0\;\;\;12u_{11}\;\;\;12u_{22}|}{18r_0\,;\;\;18r_{11}\,;\;\;4\;\;\overline{3}r_{12}\;\;\;18t_0\,;\;\;9t_{11}\,;\;\;9t_{22}\;\;\;18u_0\,;\;\;9u_{11}\,;\;\;9u_{22}\;\;\;3\varepsilon_1\,;\;\;3\varepsilon_2|^2}$$
$$\frac{6)3r_1\;\;\;3r_2\,;\;\;t_1\,;\;\;8u_1+)r_1\;\;\;r_2\,;\;\;t_1\,;\;\;2u_1+}{6r_0\;\;\;6r_{11}\;\;\;2\;\;\overline{3}r_{12}\,;\;\;6t_0\;\;\;3t_{11}\;\;\;3t_{22}\,;\;\;6u_0\;\;\;3u_{11}\;\;\;3u_{22}\,;\;\;\varepsilon_1\;\;\;\varepsilon_2}$$
$$\frac{18)3r_1\;\;\;3r_2\,;\;\;t_1\,;\;\;8u_1+)r_1\;\;\;r_2\,;\;\;t_1\,;\;\;2u_1+}{18r_0\;\;\;18r_{11}\;\;\;4\;\;\overline{3}r_{12}\,;\;\;18t_0\;\;\;9t_{11}\;\;\;9t_{22}\,;\;\;18u_0\;\;\;9u_{11}\;\;\;9u_{22}\,;\;\;3\varepsilon_1\;\;\;3\varepsilon_2}\,;\;\;9r_0\,;\;\;t_0\,;\;\;16u_0\Big\langle \tag{C11}$$
$$\sim\Big)\frac{3)r_1\;\;\;r_2\,;\;\;t_1\,;\;\;2u_1+\frac{2}{}}{6r_0\,;\;\;6r_{11}\,;\;\;2\;\;\overline{3}r_{12}\;\;\;6t_0\,;\;\;3t_{11}\,;\;\;3t_{22}\;\;\;6u_0\,;\;\;3u_{11}\,;\;\;3u_{22}\;\;\;\varepsilon_1\,;\;\;\varepsilon_2}$$
$$;\;\;\frac{9)r_1\;\;\;r_2\,;\;\;t_1\,;\;\;2u_1+\frac{2}{}}{18r_0\,;\;\;18r_{11}\,;\;\;4\;\;\overline{3}r_{12}\,;\;\;3)\;\;6t_0\,;\;\;3t_{11}\,;\;\;3t_{22}\;\;\;6u_0\,;\;\;3u_{11}\,;\;\;3u_{22}\;\;\;\varepsilon_1\,;\;\;\varepsilon_2+}\,;\;\;3r_0\,;\;\;t_0\,;\;\;4u_0\Big\langle$$
$$\sim\Big)\;\frac{3)r_1\;\;\;r_2\,;\;\;t_1\,;\;\;2u_1+\frac{2}{}}{6r_0\;\;\;6r_{11}\;\;\;2\;\;\overline{3}r_{12}\,;\;\;6t_0\;\;\;3t_{11}\;\;\;3t_{22}\,;\;\;6u_0\;\;\;3u_{11}\;\;\;3u_{22}\,;\;\;\varepsilon_1\;\;\;\varepsilon_2}$$
$$\frac{9)r_1\;\;\;r_2\,;\;\;t_1\,;\;\;2u_1+\frac{2}{}}{18r_0\;\;\;18r_{11}\;\;\;4\;\;\overline{3}r_{12}\,;\;\;18t_0\;\;\;9t_{11}\;\;\;9t_{22}\,;\;\;18u_0\;\;\;9u_{11}\;\;\;9u_{22}\,;\;\;3\varepsilon_1\;\;\;3\varepsilon_2}\,;\;\;3r_0\,;\;\;t_0\,;\;\;4u_0\Big\langle^{\;2}\;.$$

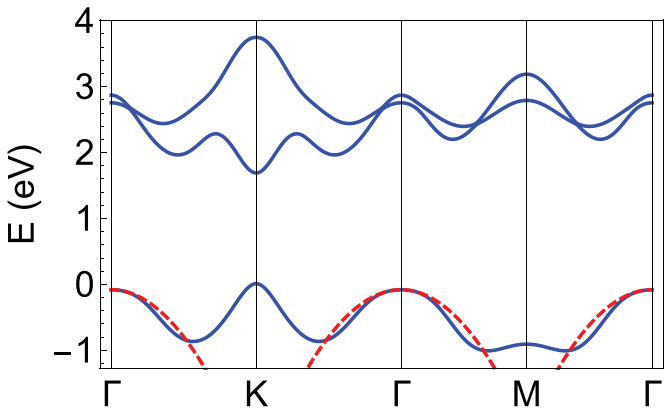

Figure 5. Plot of the band structure of WS_2 under the influence of circularly polarized light of strength $A = 0.1$ using GGA parameters from [150]. Dashed in red we see the quadratic approximation to lowest band of the Hamiltonian that is valid near the Γ point.

Since this result is very unwieldy and not very insightful, we have decided to provide numeric results for specific choices of TMDs are given in the main text in table 1.

Appendix D. Downfolding the three band model of a TMD subjected to circularly polarized light in the high frequency limit and near the *K* point

In this appendix, we study the impact of circularly polarized light on a twisted TMD hetero bilayer. We are interested in the effective mass near the K point. The starting point of our discussion, unlike near the point, is the first nearest neighbor three band tight binding model of a TMD that was derived in [150]. We chose this model because the band structure near the K point is well captured by this simpler model—unlike the bands near the point. Furthermore, it allows for more analytical progress. The model is given as below

$$H^{\mathrm{TNN}})\mathbf{k}+[\quad \left(\begin{array}{ccc} h_0 & h_1 & h_2 \\ h_1^\circ & h_{11} & h_{12} \\ h_2^\circ & h_{12}^\circ & h_{22} \end{array} \right) \sum . \tag{D1}$$

This Hamiltonian much like the third nearest neighbor model from the previous section is written in the basis of d-orbitals $\}d_{z^2}, d_{xy}, d_{x^2\ y^2}\langle$. The different contributions to the Hamiltonian are given as

$$h_0 [\quad 2t_0)\cos 2X_k ; \quad 2\cos X_k \cos Y_k +; \quad \epsilon_1 \tag{D2}$$

$$h_1 [\quad 2 \quad \overline{3}t_2 \sin X_k \sin Y_k ; \quad 2it_1)\sin 2X_k ; \quad \sin X_k \cos Y_k +\!= \tag{D3}$$

$$h_2 [\quad 2t_2)\cos 2X_k \quad \cos X_k \cos Y_k +; \quad 2i \quad \overline{3}t_1 \cos X_k \sin Y_k \tag{D4}$$

$$h_{11} [\quad 2t_{11} \cos 2X_k ; \quad)t_{11} ; \quad 3t_{22} +\cos X_k \cos Y_k ; \quad \epsilon_2 \tag{D5}$$

$$h_{22} [\quad 2t_{22} \cos 2X_k ; \quad)3t_{11} ; \quad t_{22} +\cos X_k \cos Y_k ; \quad \epsilon_2 \tag{D6}$$

$$h_{12} [\quad \overline{3})t_{22} \quad t_{11} +\sin X_k \sin Y_k ; \quad 4it_{12} \sin X_k)\cos X_k \quad \cos Y_k + \tag{D7}$$

with the shorthand

$$X_k [\quad \frac{1}{2}k_x a = \quad Y_k [\quad \frac{\overline{3}}{2}k_y a. \tag{D8}$$

The different couplings ε_i and t_i for a variety of different TMDs can be found in [150].

Circularly polarized light may be included using the same minimal coupling procedure as in the previous appendix C. We also make use of the same average Hamiltonian approach as in appendix C and find that circularly light renormalized the effective mass near the K point according to

$$\frac{m^\circ)A+}{m^\circ)0+}[\quad \frac{(\ )0+}{(\ )A+} \tag{D9}$$

with

$$\begin{aligned} \Xi(A) &= 4J_0(aA) \\ &\times \left(-\frac{6\left(t_1^2 + 2\sqrt{3}t_1 t_2 + 3t_2^2\right) J_0(aA)}{3J_0(aA)\left(-2t_0 + t_{11} + 2\sqrt{3}t_{12} + t_{22}\right) + 2(\epsilon_1 - \epsilon_2)} \right. \\ &\left. -\frac{\sqrt{3}(t_{11} - t_{22})^2}{4t_{12}} + t_{11} + 2\sqrt{3}t_{12} + t_{22} \right), \end{aligned} \tag{D10}$$

where J_0 is the 0th Bessel function of the first kind. An expansion to second order in field strength A yields the result that is referenced in the main text.

ORCID iDs

Michael Vogl https://orcid.org/0000-0003-1482-9234
Gregory A Fiete https://orcid.org/0000-0001-9477-0804

References

[1] Andrei E Y, Efetov D K, Jarillo-Herrero P, MacDonald A H, Mak K F, Senthil T, Tutuc E, Yazdani A and Young A F 2021 The marvels of moiré materials *Nat. Rev. Mater.* **6** 201–6
[2] He F, Zhou Y, Ye Z, Cho S-H, Jeong J, Meng X and Wang Y 2021 Moiré patterns in 2D materials: a review *ACS Nano* **15** 5944–58
[3] MacDonald A H 2019 Bilayer graphene's wicked, twisted road *Physics* **12** 12
[4] Zeller P and Günther S 2014 What are the possible moiré patterns of graphene on hexagonally packed surfaces? Universal solution for hexagonal coincidence lattices, derived by a geometric construction *New J. Phys.* **16** 083028
[5] Kennes D M, Claassen M, Xian L, Georges A, Millis A J, Hone J, Dean C R, Basov D, Pasupathy A N and Rubio A 2021 Moiré heterostructures as a condensed-matter quantum simulator *Nat. Phys.* **17** 155–63
[6] Bistritzer R and MacDonald A H 2011 Moiré bands in twisted double-layer graphene *Proc. Natl Acad. Sci.* **108** 12233

[7] Morell E S, Correa J, Vargas P, Pacheco M and Barticevic Z 2010 Flat bands in slightly twisted bilayer graphene: tight-binding calculations *Phys. Rev.* B **82** 121407

[8] Lopes dos Santos J M B, Peres N M R and Castro Neto A H 2012 Continuum model of the twisted graphene bilayer *Phys. Rev.* B **86** 155449

[9] Hu X, Kargarian M and Fiete G A 2011 Topological insulators and fractional quantum Hall effect on the ruby lattice *Phys. Rev.* B **84** 155116

[10] Parameswaran S A, Roy R and Sondhi S L 2013 Fractional quantum Hall physics in topological flat bands *C. R. Physique* **14** 816–39

[11] Wu Y-L, Bernevig B A and Regnault N 2012 Zoology of fractional Chern insulators *Phys. Rev.* B **85** 075116

[12] Wang F and Ran Y 2011 Nearly flat band with Chern number $c = 2$ on the dice lattice *Phys. Rev.* B **84** 241103

[13] Sun K, Gu Z, Katsura H and Das Sarma S 2011 Nearly flatbands with nontrivial topology *Phys. Rev. Lett.* **106** 236803

[14] Neupert T, Santos L, Chamon C and Mudry C 2011 Fractional quantum Hall states at zero magnetic field *Phys. Rev. Lett.* **106** 236804

[15] Tang E, Mei J-W and Wen X-G 2011 High-temperature fractional quantum Hall states *Phys. Rev. Lett.* **106** 236802

[16] Regnault N and Bernevig B A 2011 Fractional Chern insulator *Phys. Rev.* X **1** 021014

[17] Kourtis S, Neupert T, Chamon C and Mudry C 2014 Fractional Chern insulators with strong interactions that far exceed band gaps *Phys. Rev. Lett.* **112** 126806

[18] Cao Y, Fatemi V, Fang S, Watanabe K, Taniguchi T, Kaxiras E and Jarillo-Herrero P 2018 Unconventional superconductivity in magic-angle graphene superlattices *Nature* **556** 43–50

[19] Vahedi J, Peters R, Missaoui A, Honecker A and de Laissardière G T 2021 Magnetism of magic-angle twisted bilayer graphene *SciPost Phys.* **11** 83

[20] Xie Y, Pierce A T, Park J M, Parker D E, Khalaf E, Ledwith P, Cao Y, Lee S H, Chen S and Forrester P R *et al* 2021 Fractional Chern insulators in magic-angle twisted bilayer graphene *Nature* **600** 439–43

[21] Cao Y, Rodan-Legrain D, Rubies-Bigorda O, Park J M, Watanabe K, Taniguchi T and Jarillo-Herrero P 2020 Tunable correlated states and spin-polarized phases in twisted bilayer–bilayer graphene *Nature* **583** 215–20

[22] Wilhelm P, Lang T C and Läuchli A M 2021 Interplay of fractional Chern insulator and charge density wave phases in twisted bilayer graphene *Phys. Rev.* B **103** 125406

[23] Rademaker L and Mellado P 2018 Charge-transfer insulation in twisted bilayer graphene *Phys. Rev.* B **98** 235158

[24] Yankowitz M, Chen S, Polshyn H, Zhang Y, Watanabe K, Taniguchi T, Graf D, Young A F and Dean C R 2019 Tuning superconductivity in twisted bilayer graphene *Science* **363** 1059–64

[25] Choi Y, Kemmer J, Peng Y, Thomson A, Arora H, Polski R, Zhang Y, Ren H, Alicea J and Refael G *et al* 2019 Electronic correlations in twisted bilayer graphene near the magic angle *Nat. Phys.* **15** 1174–80

[26] Sherkunov Y and Betouras J J 2018 Electronic phases in twisted bilayer graphene at magic angles as a result of Van Hove singularities and interactions *Phys. Rev.* B **98** 205151

[27] Xie M and MacDonald A H 2020 Nature of the correlated insulator states in twisted bilayer graphene *Phys. Rev. Lett.* **124** 097601

[28] Codecido E *et al* 2019 Correlated insulating and superconducting states in twisted bilayer graphene below the magic angle *Sci. Adv.* **5** eaaw9770

[29] Wong D, Nuckolls K P, Oh M, Lian B, Xie Y, Jeon S, Watanabe K, Taniguchi T, Bernevig B A and Yazdani A 2020 Cascade of electronic transitions in magic-angle twisted bilayer graphene *Nature* **582** 198–202

[30] Lu X *et al* 2019 Superconductors, orbital magnets and correlated states in magic-angle bilayer graphene *Nature* **574** 653–7

[31] Sharpe A L, Fox E J, Barnard A W, Finney J, Watanabe K, Taniguchi T, Kastner M A and Goldhaber-Gordon D 2019 Emergent ferromagnetism near three-quarters filling in twisted bilayer graphene *Science* **365** 605–8

[32] Seo K, Kotov V N and Uchoa B 2019 Ferromagnetic Mott state in twisted graphene bilayers at the magic angle *Phys. Rev. Lett.* **122** 246402

[33] Tran K *et al* 2019 Evidence for moiré excitons in van der Waals heterostructures *Nature* **567** 71–75

[34] Seyler K L, Rivera P, Yu H, Wilson N P, Ray E L, Mandrus D G, Yan J, Yao W and Xu X 2019 Signatures of moiré-trapped valley excitons in $MoSe_2/WSe_2$ heterobilayers *Nature* **567** 66–70

[35] Alexeev E M *et al* 2019 Resonantly hybridized excitons in moiré superlattices in van der Waals heterostructures *Nature* **567** 81–86

[36] Hu N C and MacDonald A H 2021 Competing magnetic states in transition metal dichalcogenide moiré materials *Phys. Rev.* B **104** 214403

[37] Wu F, Lovorn T, Tutuc E and MacDonald A H 2018 Hubbard model physics in transition metal dichalcogenide moiré bands *Phys. Rev. Lett.* **121** 026402

[38] Morales-Duràn N, Hu N C, Potasz P and MacDonald A H 2021 Non-local interactions in moiré Hubbard systems (arXiv:2108.03313 [cond-mat.str-el])

[39] Wu F, Lovorn T, Tutuc E, Martin I and MacDonald A H 2019 Topological insulators in twisted transition metal dichalcogenide homobilayers *Phys. Rev. Lett.* **122** 086402

[40] Tang Y *et al* 2020 Simulation of Hubbard model physics in WSe_2/WS_2 moiré superlattices *Nature* **579** 353–8

[41] Zare M-H and Mosadeq H 2021 Spin liquid in twisted homobilayers of group-VI dichalcogenides *Phys. Rev.* B **104** 115154

[42] Andersen T I *et al* 2021 Excitons in a reconstructed moiré potential in twisted WSe_2/WSe_2 homobilayers *Nat. Mater.* **20** 480–7

[43] Wang L *et al* 2020 Correlated electronic phases in twisted bilayer transition metal dichalcogenides *Nat. Mater.* **19** 861–6

[44] Angeli M and MacDonald A H 2021 Γ valley transition metal dichalcogenide moiré bands *Proc. Natl Acad. Sci.* **118** e2021826118

[45] Navarro-Labastida L A, Espinosa-Champo A, Aguilar-Mendez E and Naumis G G 2022 Why the first magic-angle is different from others in twisted graphene bilayers: interlayer currents, kinetic and confinement energy and wave-function localization *Phys. Rev.* B **105** 115434

[46] Naumis G G, Navarro-Labastida L A, Aguilar-Méndez E and Espinosa-Champo A 2021 Reduction of the twisted bilayer graphene chiral Hamiltonian into a 2×2 matrix operator and physical origin of flat bands at magic angles *Phys. Rev.* B **103** 245418

[47] Mirzakhani M, Peeters F M and Zarenia M 2020 Circular quantum dots in twisted bilayer graphene *Phys. Rev.* B **101** 075413

[48] Fleischmann M, Gupta R, Wullschläger F, Theil S, Weckbecker D, Meded V, Sharma S, Meyer B and Shallcross S 2019 Perfect and controllable nesting in minimally twisted bilayer graphene *Nano Lett.* **20** 971–8

[49] Vogl M, Pankratov O and Shallcross S 2017 Semiclassics for matrix Hamiltonians: the Gutzwiller trace formula with applications to graphene-type systems *Phys. Rev.* B **96** 035442

[50] Abanin D A, De Roeck W, Ho W W and Huveneers F M C 2017 Effective Hamiltonians, prethermalization and slow energy absorption in periodically driven many-body systems *Phys. Rev.* B **95** 014112

[51] Vajna S, Klobas K, Prosen T and Polkovnikov A 2018 Replica resummation of the Baker-Campbell-Hausdorff series *Phys. Rev. Lett.* **120** 200607

[52] Blanes S, Casas F, Oteo J and Ros J 2009 The Magnus expansion and some of its applications *Phys. Rep.* **470** 151–238

[53] Rahav S, Gilary I and Fishman S 2003 Effective Hamiltonians for periodically driven systems *Phys. Rev.* A **68** 013820

[54] Rahav S, Gilary I and Fishman S 2003 Time independent description of rapidly oscillating potentials *Phys. Rev. Lett.* **91** 110404

[55] Bukov M, D'Alessio L and Polkovnikov A 2015 Universal high-frequency behavior of periodically driven systems: from dynamical stabilization to Floquet engineering *Adv. Phys.* **64** 139–226

[56] Eckardt A and Anisimovas E 2015 High-frequency approximation for periodically driven quantum systems from a Floquet-space perspective *New J. Phys.* **17** 093039

[57] Fel'dman E 1984 On the convergence of the Magnus expansion for spin systems in periodic magnetic fields *Phys. Lett.* A **104** 479–81

[58] Magnus W 1954 On the exponential solution of differential equations for a linear operator *Commun. Pure Appl. Math.* **7** 649–73

[59] Goldman N and Dalibard J 2014 Periodically driven quantum systems: effective Hamiltonians and engineered gauge fields *Phys. Rev.* X **4** 031027

[60] Itin A P and Katsnelson M I 2015 Effective Hamiltonians for rapidly driven many-body lattice systems: induced exchange interactions and density-dependent hoppings *Phys. Rev. Lett.* **115** 075301

[61] Mikami T, Kitamura S, Yasuda K, Tsuji N, Oka T and Aoki H 2016 Brillouin-Wigner theory for high-frequency expansion in periodically driven systems: application to Floquet topological insulators *Phys. Rev.* B **93** 144307

[62] Mohan P, Saxena R, Kundu A and Rao S 2016 Brillouin-Wigner theory for Floquet topological phase transitions in spin-orbit-coupled materials *Phys. Rev.* B **94** 235419

[63] Bukov M, Kolodrubetz M and Polkovnikov A 2016 Schrieffer-Wolff transformation for periodically driven systems: strongly correlated systems with artificial gauge fields *Phys. Rev. Lett.* **116** 125301

[64] Vogl M, Laurell P, Barr A D and Fiete G A 2019 Analog of Hamilton-Jacobi theory for the time-evolution operator *Phys. Rev.* A **100** 012132

[65] Verdeny A, Mielke A and Mintert F 2013 Accurate effective Hamiltonians via unitary flow in Floquet space *Phys. Rev. Lett.* **111** 175301

[66] Gómez-León A and Platero G 2013 Floquet-Bloch theory and topology in periodically driven lattices *Phys. Rev. Lett.* **110** 200403

[67] Vogl M, Rodriguez-Vega M and Fiete G A 2020 Effective Floquet Hamiltonian in the low-frequency regime *Phys. Rev.* B **101** 024303

[68] Vogl M, Laurell P, Barr A D and Fiete G A 2019 Flow equation approach to periodically driven quantum systems *Phys. Rev.* X **9** 021037

[69] Rodriguez-Vega M, Lentz M and Seradjeh B 2018 Floquet perturbation theory: formalism and application to low-frequency limit *New J. Phys.* **20** 093022

[70] Rodriguez-Vega M and Seradjeh B 2018 Universal fluctuations of Floquet topological invariants at low frequencies *Phys. Rev. Lett.* **121** 036402

[71] Martiskainen H and Moiseyev N 2015 Perturbation theory for quasienergy Floquet solutions in the low-frequency regime of the oscillating electric field *Phys. Rev.* A **91** 023416

[72] Rigolin G, Ortiz G and Ponce V H 2008 Beyond the quantum adiabatic approximation: adiabatic perturbation theory *Phys. Rev.* A **78** 052508

[73] Weinberg M, Ölschläger C, Sträter C, Prelle S, Eckardt A, Sengstock K and Simonet J 2015 Multiphoton interband excitations of quantum gases in driven optical lattices *Phys. Rev.* A **92** 043621

[74] Li Z-Z, Lam C-H and You J Q 2017 Floquet engineering of long-range *p*-wave superconductivity: beyond the high-frequency limit *Phys. Rev.* B **96** 155438

[75] Kennes D M, Müller N, Pletyukhov M, Weber C, Bruder C, Hassler F, Klinovaja J, Loss D and Schoeller H 2019 Chiral one-dimensional Floquet topological insulators beyond the rotating wave approximation *Phys. Rev.* B **100** 041103

[76] Müller N, Kennes D M, Klinovaja J, Loss D and Schoeller H 2020 Electronic transport in one-dimensional Floquet topological insulators via topological and nontopological edge states *Phys. Rev.* B **101** 155417

[77] Novicenko V, Žlabys G and Anisimovas E 2021 Flow-equation approach to quantum systems driven by an amplitude-modulated time-periodic force (arXiv:2111.15368 [quant-ph])

[78] Shirai T, Thingna J, Mori T, Denisov S, Hänggi P and Miyashita S 2016 Effective Floquet–Gibbs states for dissipative quantum systems *New J. Phys.* **18** 053008

[79] Ikeda T N, Chinzei K and Sato M 2021 Nonequilibrium steady states in the Floquet-Lindblad systems: van Vleck's high-frequency expansion approach *SciPost Phys. Core* **4** 33

[80] Ikeda T N and Polkovnikov A 2021 Fermi's golden rule for heating in strongly driven Floquet systems *Phys. Rev.* B **104** 134308

[81] Engelhardt G, Platero G and Cao J 2019 Discontinuities in driven spin-boson systems due to coherent destruction of tunneling: breakdown of the Floquet-Gibbs distribution *Phys. Rev. Lett.* **123** 120602

[82] Basov D N, Averitt R D and Hsieh D 2017 Towards properties on demand in quantum materials *Nat. Mater.* **16** 1077

[83] Oka T and Kitamura S 2019 Floquet engineering of quantum materials *Annu. Rev. Condens. Matter Phys.* **10** 387–408

[84] Rudner M S and Lindner N H 2020 Band structure engineering and non-equilibrium dynamics in Floquet topological insulators *Nat. Rev. Phys.* **2** 229–44

[85] Giovannini U D and Hübener H 2019 Floquet analysis of excitations in materials *J. Phys.: Mater.* **3** 012001

[86] McIver J W, Schulte B, Stein F-U, Matsuyama T, Jotzu G, Meier G and Cavalleri A 2020 Light-induced anomalous Hall effect in graphene *Nat. Phys.* **16** 38–41

[87] Oka T and Aoki H 2009 Photovoltaic Hall effect in graphene *Phys. Rev.* B **79** 081406

[88] Lindner N H, Refael G and Galitski V 2011 Floquet topological insulator in semiconductor quantum wells *Nat. Phys.* **7** 490–5

[89] Rechtsman M C, Zeuner J M, Plotnik Y, Lumer Y, Podolsky D, Dreisow F, Nolte S, Segev M and Szameit A 2013 Photonic Floquet topological insulators *Nature* **496** 196–200

[90] Rudner M S, Lindner N H, Berg E and Levin M 2013 Anomalous edge states and the bulk-edge correspondence for periodically driven two-dimensional systems *Phys. Rev.* X **3** 031005

[91] Inoue J-I and Tanaka A 2010 Photoinduced transition between conventional and topological insulators in

two-dimensional electronic systems *Phys. Rev. Lett.* **105** 017401
[92] Peng Y and Refael G 2019 Floquet second-order topological insulators from nonsymmorphic space-time symmetries *Phys. Rev. Lett.* **123** 016806
[93] Huang B and Liu W V 2020 Floquet higher-order topological insulators with anomalous dynamical polarization *Phys. Rev. Lett.* **124** 216601
[94] Bomantara R W, Zhou L, Pan J and Gong J 2019 Coupled-wire construction of static and Floquet second-order topological insulators *Phys. Rev.* B **99** 045441
[95] Peng Y 2020 Floquet higher-order topological insulators and superconductors with space-time symmetries *Phys. Rev. Res.* **2** 013124
[96] Pan J and Zhou L 2020 Non-Hermitian Floquet second order topological insulators in periodically quenched lattices *Phys. Rev.* B **102** 094305
[97] Chaudhary S, Haim A, Peng Y and Refael G 2020 Phonon-induced Floquet topological phases protected by space-time symmetries *Phys. Rev. Res.* **2** 043431
[98] Hu H, Huang B, Zhao E and Liu W V 2020 Dynamical singularities of Floquet higher-order topological insulators *Phys. Rev. Lett.* **124** 057001
[99] Kennes D M, de la Torre A, Ron A, Hsieh D and Millis A J 2018 Floquet engineering in quantum chains *Phys. Rev. Lett.* **120** 127601
[100] D'Alessio L and Rigol M 2014 Long-time behavior of isolated periodically driven interacting lattice systems *Phys. Rev.* X **4** 041048
[101] Harper F and Roy R 2017 Floquet topological order in interacting systems of bosons and fermions *Phys. Rev. Lett.* **118** 115301
[102] Reiss D, Harper F and Roy R 2018 Interacting Floquet topological phases in three dimensions *Phys. Rev.* B **98** 045127
[103] von Keyserlingk C W and Sondhi S L 2016 Phase structure of one-dimensional interacting Floquet systems. I. Abelian symmetry-protected topological phases *Phys. Rev.* B **93** 245145
[104] Kennes D M, Claassen M, Sentef M A and Karrasch C 2019 Light-induced *d*-wave superconductivity through Floquet-engineered Fermi surfaces in cuprates *Phys. Rev.* B **100** 075115
[105] Dóra B, Cayssol J, Simon F and Moessner R 2012 Optically engineering the topological properties of a spin Hall insulator *Phys. Rev. Lett.* **108** 056602
[106] Decker K S C, Karrasch C, Eisert J and Kennes D M 2020 Floquet engineering topological many-body localized systems *Phys. Rev. Lett.* **124** 190601
[107] Zhang L, Khemani V and Huse D A 2016 A Floquet model for the many-body localization transition *Phys. Rev.* B **94** 224202
[108] Abanin D A, De Roeck W and Huveneers F 2016 Theory of many-body localization in periodically driven systems *Ann. Phys., NY* **372** 1–11
[109] Ponte P, Papić Z, Huveneers F M C and Abanin D A 2015 Many-body localization in periodically driven systems *Phys. Rev. Lett.* **114** 140401
[110] Abanin D A, Altman E, Bloch I and Serbyn M 2019 Colloquium: Many-body localization, thermalization and entanglement *Rev. Mod. Phys.* **91** 021001
[111] Dal Lago V, Atala M and Foa Torres L E F 2015 Floquet topological transitions in a driven one-dimensional topological insulator *Phys. Rev.* A **92** 023624
[112] Calvo H L, Foa Torres L E F, Perez-Piskunow P M, Balseiro C A and Usaj G 2015 Floquet interface states in illuminated three-dimensional topological insulators *Phys. Rev.* B **91** 241404
[113] Asbóth J K, Tarasinski B and Delplace P 2014 Chiral symmetry and bulk-boundary correspondence in periodically driven one-dimensional systems *Phys. Rev.* B **90** 125143
[114] Calvo H L, Pastawski H M, Roche S and Torres L E F F 2011 Tuning laser-induced band gaps in graphene *Appl. Phys. Lett.* **98** 232103
[115] Rodriguez-Vega M, Vogl M and Fiete G A 2021 Direct driving of electronic and phononic degrees of freedom in a honeycomb bilayer with infrared light *Phys. Rev.* B **104** 245135
[116] Gu Z, Fertig H A, Arovas D P and Auerbach A 2011 Floquet spectrum and transport through an irradiated graphene ribbon *Phys. Rev. Lett.* **107** 216601
[117] Syzranov S V, Rodionov Y I, Kugel K I and Nori F 2013 Strongly anisotropic dirac quasiparticles in irradiated graphene *Phys. Rev.* B **88** 241112
[118] Perez-Piskunow P M, Usaj G, Balseiro C A and Torres L E F F 2014 Floquet chiral edge states in graphene *Phys. Rev.* B **89** 121401
[119] Kundu A, Fertig H A and Seradjeh B 2014 Effective theory of Floquet topological transitions *Phys. Rev. Lett.* **113** 236803
[120] Sentef M A, Claassen M, Kemper A F, Moritz B, Oka T, Freericks J K and Devereaux T P 2015 Theory of Floquet band formation and local pseudospin textures in pump-probe photoemission of graphene *Nat. Commun.* **6** 7047
[121] Roman-Taboada P and Naumis G G 2017 Topological flat bands in time-periodically driven uniaxial strained graphene nanoribbons *Phys. Rev.* B **95** 115440
[122] Dehghani H, Oka T and Mitra A 2015 Out-of-equilibrium electrons and the Hall conductance of a Floquet topological insulator *Phys. Rev.* B **91** 155422
[123] Kitagawa T, Oka T, Brataas A, Fu L and Demler E 2011 Transport properties of nonequilibrium systems under the application of light: photoinduced quantum Hall insulators without landau levels *Phys. Rev.* B **84** 235108
[124] Usaj G, Perez-Piskunow P M, Foa Torres L E F and Balseiro C A 2014 Irradiated graphene as a tunable Floquet topological insulator *Phys. Rev.* B **90** 115423
[125] Perez-Piskunow P M, Foa Torres L E F and Usaj G 2015 Hierarchy of Floquet gaps and edge states for driven honeycomb lattices *Phys. Rev.* A **91** 043625
[126] Bhattacharya U, Chaudhary S, Grass T, Johnson A S, Wall S and Lewenstein M 2022 Fermionic Chern insulator from twisted light with linear polarization *Phys. Rev.* B **105** L081406
[127] Mentink J H and Eckstein M 2014 Ultrafast quenching of the exchange interaction in a Mott insulator *Phys. Rev. Lett.* **113** 057201
[128] Mentink J, Balzer K and Eckstein M 2015 Ultrafast and reversible control of the exchange interaction in Mott insulators *Nat. Commun.* **6** 1–8
[129] Mentink J 2017 Manipulating magnetism by ultrafast control of the exchange interaction *J. Phys.: Condens. Matter* **29** 453001
[130] Liu J, Hejazi K and Balents L 2018 Floquet engineering of multiorbital Mott insulators: applications to orthorhombic titanates *Phys. Rev. Lett.* **121** 107201
[131] Hejazi K, Liu J and Balents L 2019 Floquet spin and spin-orbital Hamiltonians and doublon-holon generations in periodically driven Mott insulators *Phys. Rev.* B **99** 205111
[132] Quito V L and Flint R 2021 Floquet engineering correlated materials with unpolarized light *Phys. Rev. Lett.* **126** 177201
[133] Quito V L and Flint R 2021 Polarization as a tuning parameter for Floquet engineering: magnetism in the

honeycomb, square and triangular Mott insulators *Phys. Rev.* B **103** 134435
[134] Chaudhary S, Hsieh D and Refael G 2019 Orbital Floquet engineering of exchange interactions in magnetic materials *Phys. Rev.* B **100** 220403
[135] Chaudhary S, Ron A, Hsieh D and Refael G 2020 Controlling ligand-mediated exchange interactions in periodically driven magnetic materials (arXiv:2009.00813)
[136] Rodriguez-Vega M, Vogl M and Fiete G A 2021 Low-frequency and moiré–Floquet engineering: a review *Ann. Phys., NY* **435** 168434
[137] Bao C, Tang P, Sun D and Zhou S 2022 Light-induced emergent phenomena in 2D materials and topological materials *Nat. Rev. Phys.* **4** 1–16
[138] Assi I A, LeBlanc J P F, Rodriguez-Vega M, Bahlouli H and Vogl M 2021 Floquet engineering and nonequilibrium topological maps in twisted trilayer graphene *Phys. Rev.* B **104** 195429
[139] Vogl M, Rodriguez-Vega M, Flebus B, MacDonald A H and Fiete G A 2021 Floquet engineering of topological transitions in a twisted transition metal dichalcogenide homobilayer *Phys. Rev.* B **103** 014310
[140] Topp G E, Eckhardt C J, Kennes D M, Sentef M A and Törmä P 2021 Light-matter coupling and quantum geometry in moiré materials *Phys. Rev.* B **104** 064306
[141] Topp G E, Jotzu G, McIver J W, Xian L, Rubio A and Sentef M A 2019 Topological Floquet engineering of twisted bilayer graphene *Phys. Rev. Res.* **1** 023031
[142] Lu M, Zeng J, Liu H, Gao J-H and Xie X C 2021 Valley-selective Floquet Chern flat bands in twisted multilayer graphene *Phys. Rev.* B **103** 195146
[143] Rodriguez-Vega M, Vogl M and Fiete G A 2020 Floquet engineering of twisted double bilayer graphene *Phys. Rev. Res.* **2** 033494
[144] Vogl M, Rodriguez-Vega M and Fiete G A 2020 Effective Floquet Hamiltonians for periodically driven twisted bilayer graphene *Phys. Rev.* B **101** 235411
[145] Vogl M, Rodriguez-Vega M and Fiete G A 2020 Floquet engineering of interlayer couplings: tuning the magic angle of twisted bilayer graphene at the exit of a waveguide *Phys. Rev.* B **101** 241408
[146] Katz O, Refael G and Lindner N H 2020 Optically induced flat bands in twisted bilayer graphene *Phys. Rev.* B **102** 155123
[147] Li Y, Fertig H A and Seradjeh B 2020 Floquet-engineered topological flat bands in irradiated twisted bilayer graphene *Phys. Rev. Res.* **2** 043275
[148] Ge R-C and Kolodrubetz M 2021 Floquet engineering of lattice structure and dimensionality in twisted moiré heterobilayers (arXiv:2103.09874)
[149] Pan H, Wu F and Das Sarma S 2020 Quantum phase diagram of a moiré-Hubbard model *Phys. Rev.* B **102** 201104
[150] Liu G-B, Shan W-Y, Yao Y, Yao W and Xiao D 2013 Three-band tight-binding model for monolayers of group-VIB transition metal dichalcogenides *Phys. Rev.* B **88** 085433
[151] Ye B, Machado F, White C D, Mong R S K and Yao N Y 2020 Emergent hydrodynamics in nonequilibrium quantum systems *Phys. Rev. Lett.* **125** 030601
[152] Weinberg P, Bukov M, D'Alessio L, Polkovnikov A, Vajna S and Kolodrubetz M 2017 Adiabatic perturbation theory and geometry of periodically-driven systems *Phys. Rep.* **688** 1–35
[153] Shan J-Y, Ye M, Chu H, Lee S, Park J-G, Balents L and Hsieh D 2021 Giant modulation of optical nonlinearity by Floquet engineering *Nature* **600** 235–9
[154] Chaudhary S, Lewandowski C and Refael G 2022 Shift-current response as a probe of quantum geometry and electron-electron interactions in twisted bilayer graphene *Phys. Rev. Res.* **4** 013164
[155] Kaplan D, Holder T and Yan B 2021 Momentum shift current at terahertz frequencies in twisted bilayer graphene (arXiv:2101.07539)
[156] Liu J and Dai X 2020 Anomalous Hall effect, magneto-optical properties and nonlinear optical properties of twisted graphene systems *npj Comput. Mater.* **6** 1–10
[157] Xu J, Zhang J, Zhang W and Lee C-S 2017 Interlayer nanoarchitectonics of two-dimensional transition-metal dichalcogenides nanosheets for energy storage and conversion applications *Adv. Energy Mater.* **7** 1700571
[158] Li M, Shi J, Liu L, Yu P, Xi N and Wang Y 2016 Experimental study and modeling of atomic-scale friction in zigzag and armchair lattice orientations of MoS_2 *Sci. Technol. Adv. Mater.* **17** 189–99
[159] Schutte W, De Boer J and Jellinek F 1987 Crystal structures of tungsten disulfide and diselenide *J. Solid State Chem.* **70** 207–9